

Optimizing Temperature Distributions for Training Neural Quantum States using Parallel Tempering

Conor Smith,^{1,2,3} Quinn T. Campbell,⁴ and Tameem Albash⁴

¹*Center for Quantum Information and Control, University of New Mexico,
University of New Mexico, Albuquerque, NM, USA*

²*Department of Electrical and Computer Engineering,
University of New Mexico, Albuquerque, NM, USA*

³*Center for Computational Quantum Physics, Flatiron Institute, New York, NY, 10010, USA*

⁴*Center for Computing Research, Sandia National Laboratories, Albuquerque NM, 87185 USA*

Parameterized artificial neural networks (ANNs) can be very expressive ansatzes for variational algorithms, reaching state-of-the-art energies on many quantum many-body Hamiltonians. Nevertheless, the training of the ANN can be slow and stymied by the presence of local minima in the parameter landscape. One approach to mitigate this issue is to use parallel tempering methods, and in this work we focus on the role played by the temperature distribution of the parallel tempering replicas. Using an adaptive method that adjusts the temperatures in order to equate the exchange probability between neighboring replicas, we show that this temperature optimization can significantly increase the success rate of the variational algorithm with negligible computational cost by eliminating bottlenecks in the replicas' random walk. We demonstrate this using two different neural networks, a restricted Boltzmann machine and a feedforward network, which we use to study a toy problem based on a permutation invariant Hamiltonian with a pernicious local minimum and the J_1 - J_2 model on a rectangular lattice.

I. INTRODUCTION

Finding or approximating the ground state of a many-body quantum Hamiltonian is an optimization problem at the core of understanding many scientifically relevant systems, such as strongly-correlated materials, quantum chemistry, and high energy physics. A standard approach to tackling this problem is applying the variational method to a parameterized wavefunction. An exact representation is generally too costly at physically relevant system sizes, so a practical representation needs to be efficient in terms of the number of its parameters but expressive enough to capture the ground state to the desired accuracy. Furthermore, the representations should be paired with an efficient algorithm to perform updates to the parameterized wavefunction. The approach is then practical if the solution is found in a total number of updates to the parameterized wavefunction that is not prohibitive. While we should not expect any single approach to be efficient for all Hamiltonian problems [1–5], new representations and algorithmic developments can help grow the number and size of Hamiltonians that can be tackled using classical computing [6–13].

The flexibility of artificial neural networks (ANNs) has made them an attractive choice for parameterized wavefunctions that can be trained using variational Monte Carlo (VMC) methods, such as stochastic reconfiguration (SR) [14, 15] and minimum-step stochastic reconfiguration [16], to approximate ground states [17]. An ANN used to represent a quantum state is now commonly referred to as a Neural Quantum State (NQS). State-of-the-art results can be achieved by carefully choosing the ANN architecture to reproduce the symmetries of the Hamiltonian of interest [18, 19]. For recent reviews of NQSs and their applications, see Ref. [20–22]. Despite the success

and promise of NQSs, training these networks to approximate the ground state can still be resource intensive [23], with the primary culprits being frustration and the sign structure of the ground state [24–26].

In this work, we continue the development of using parallel tempering (PT) [27–29] as a metaheuristic for training NQSs [30]. By simulating multiple systems in parallel, with each operating at a different temperature, PT aims to overcome barriers in the energy landscape by allowing systems to be kicked to higher temperatures where they can escape local minima and then relax back to colder temperatures and reach lower energy configurations. Here we focus on the role played by the temperature distribution of the replicas, known to play an important role in the efficiency of PT in the study of spin glasses [31]. By using an adaptive method for optimizing the temperature distribution of replicas, we demonstrate an improvement in the success frequency beyond what is achieved with PT without the adaptive temperature.

The manuscript is organized as follows. In Sec. II, we describe our methodology, including the ANN architectures, variational algorithms, and PT method used. In Sec. III, we present our results for the two classes of problems we study, the Precipice problem and the J_1 - J_2 model. The Precipice problem has an energy landscape that drives the training to a local minimum from which it is very difficult to escape and serves as a useful toy model to demonstrate how our temperature optimization can improve performance. Because of its simplicity, we study this model with only a Restricted Boltzmann Machine (RBM) [32, 33]. For the J_1 - J_2 model, we use both a RBM and a feedforward [34] network architecture in order to illustrate the usefulness of our methods on different architectures. In Sec. IV, we discuss our results and conclusions.

II. THE SETUP

A. Wavefunction Representation

We define our (unnormalized) parameterized wavefunction $|\psi(\alpha)\rangle$ as:

$$|\psi(\alpha)\rangle = \sum_{x \in \{0,1\}^{\otimes n}} \psi_x(\alpha)|x\rangle, \quad (1)$$

where the set $\{|x\rangle\}_x$ is the computational basis for n qubits¹. The function $\psi_x(\alpha)$ is the output of an ANN with parameters $\{\alpha_k\}_k$ given the input x . In this work, we focus on two types of ANN's, the Restricted Boltzmann Machine (RBM) and a three layer feedforward neural network. For a RBM with n visible nodes and m hidden nodes, the parameterized function is given by:

$$\psi_x(\alpha) = e^{\sum_{i=1}^n a_i z_i} \prod_{\mu=1}^m \cosh \left(b_\mu + \sum_{k=1}^n W_{\mu k} z_k \right), \quad (2)$$

where $z_i = 1 - 2x_i$ and where we have expressed the $(n + m + nm)$ complex parameters α in terms of the complex set $\{a_i, b_\mu, W_{\mu k}\}$.

On larger Hamiltonian systems with a more complex ground state structure, it is advantageous to use a deeper network, so we add two layers to the above construction to form our three layer feedforward ANN. In this case, the output of the ANN can be expressed as

$$\psi_x(\alpha) = \phi_h^{(2)}(\phi_h^{(1)}(\phi_v(z_i))), \quad (3)$$

where $\phi_v^{(h)} = \sigma(W_{ji}^{v(h)} z_i)$ is the visible (hidden) layer with the learnable weight matrix $W^{v(h)}$ and activation function σ . All activation functions are Gaussian Error Linear Unit (GELU) functions [35] defined as:

$$\sigma(x) = \frac{x}{2} \left(1 + \operatorname{erf} \left(\frac{x}{\sqrt{2}} \right) \right), \quad (4)$$

where $\operatorname{erf}(x)$ is the Gauss error function.

The RBM construction allows for outputs and gradients to be computed directly. For the feedforward and more general structures, auto-differentiation is convenient to compute gradients. We therefore implement the feedforward network in the NQS VMC package NetKet [36, 37], which is built on JAX [38] and allows the use of arbitrary network structures.

B. Optimizing the Free Energy

In our work, the target of the training of the ANN's is to minimize a cost function that is akin to the free energy

$$F(\alpha, \alpha^*) = \frac{\langle \psi(\alpha) | \hat{H} | \psi(\alpha) \rangle}{\langle \psi(\alpha) | \psi(\alpha) \rangle} - TS(\alpha, \alpha^*), \quad (5)$$

where T is the temperature of the replica and $S(\alpha, \alpha^*)$ is the von-Neumann entropy of the probability distribution associated with measurements in the computational basis:

$$S(\alpha, \alpha^*) = - \sum_x p_x(\alpha, \alpha^*) \ln p_x(\alpha, \alpha^*), \quad (6)$$

where $p_x(\alpha, \alpha^*) = \frac{|\langle x | \psi(\alpha) \rangle|^2}{\langle \psi(\alpha) | \psi(\alpha) \rangle}$. Training with this cost function was used in Refs. [19, 39] in the context of annealing but here we use it in the context of our PT scheme (see also Ref. [30] for an alternative to the free energy).

To see how introducing the entropy term to the cost function changes the update rule for SR (see Appendix A of Ref. [30] for a derivation), we can expand Eq. (5) to first order in the perturbations to the parameters α and α^* . We have:

$$\begin{aligned} F(\alpha + \delta\alpha, \alpha^* + \delta\alpha^*) &= F(\alpha, \alpha^*) \\ &+ \sum_k \left(\delta\alpha_k^* \frac{\langle \psi(\alpha) | (\hat{O}_k^\dagger - \langle \hat{O}_k^\dagger \rangle) \hat{F}(\alpha, \alpha^*) | \psi(\alpha) \rangle}{\langle \psi(\alpha) | \psi(\alpha) \rangle} \right. \\ &\quad \left. + \delta\alpha_k \frac{\langle \psi(\alpha) | \hat{F}(\alpha, \alpha^*) (\hat{O}_k - \langle \hat{O}_k \rangle) | \psi(\alpha) \rangle}{\langle \psi(\alpha) | \psi(\alpha) \rangle} + \dots \right), \end{aligned} \quad (7)$$

where we defined the parameter-dependent operators:

$$\hat{F}(\alpha, \alpha^*) = \hat{H} - T\hat{S}(\alpha, \alpha^*), \quad (8a)$$

$$\hat{S}(\alpha, \alpha^*) = - \sum_x \ln(|\psi_x(\alpha)|^2) |x\rangle\langle x|, \quad (8b)$$

$$\hat{O}_k(\alpha) = \sum_x \frac{1}{\psi_x(\alpha)} \frac{\partial}{\partial \alpha_k} \psi_x(\alpha) |x\rangle\langle x|, \quad (8c)$$

and the expectation value of an operator \hat{A} is defined as:

$$\langle \hat{A} \rangle = \frac{\langle \psi(\alpha) | \hat{A} | \psi(\alpha) \rangle}{\langle \psi(\alpha) | \psi(\alpha) \rangle}. \quad (9)$$

Minimizing the free energy $F(\alpha, \alpha^*)$ using SR amounts to performing the updates

$$\delta\alpha_k = -\eta \sum_{k'} s_{kk'}^{-1} f_{k'}, \quad (10)$$

where η is the learning rate and where the force vector f_k and covariance matrix $s_{kk'}$ are defined as (suppressing the dependence on α, α^*):

$$f_k = \langle \hat{O}_k^\dagger \hat{F} \rangle - \langle \hat{O}_k^\dagger \rangle \langle \hat{F} \rangle, \quad (11a)$$

$$s_{kk'} = \langle \hat{O}_k^\dagger \hat{O}_{k'} \rangle - \langle \hat{O}_k^\dagger \rangle \langle \hat{O}_{k'} \rangle. \quad (11b)$$

Thus the introduction of the entropy term amounts to replacing the local energy that appears in the force vector with the local energy plus $T \ln(|\psi_x(\alpha)|^2)$ [19].

¹ We pick the convention that for the Pauli z operator on a single qubit, the computational basis satisfies $\sigma^z|0\rangle = |0\rangle$ and $\sigma^z|1\rangle = -|1\rangle$.

C. Parallel Tempering and Optimizing the swap probability

In order to help the training of our ANN's escape from local minima, we implement PT [27–29] as part of our optimization. Details of the adaptation of the method to training ANN's are provided in Ref. [30], but we provide a summary here for completeness.

Multiple ANN's, each called a replica, are trained in parallel with SR. The i -th replica is trained using a unique temperature T_i as described in Sec. II B, with the 0-th replica set at zero temperature. After a fix number of SR updates, a configuration swap of neighboring replicas is attempted with probability

$$p_{i,i+1} = \min(1, \exp[(\beta_i - \beta_{i+1})(\bar{E}_i - \bar{E}_{i+1})]) \quad (12)$$

for $i \in [0, n_R - 2]$ and where $\beta_i = 1/T_i$ is the inverse temperature and \bar{E}_i is a running average of the expectation value $\langle \hat{H} \rangle$. In our implementation of PT, we attempt neighbor swaps between i even and $i + 1$ odd replicas after n_{swap} SR updates, and then attempt neighbor swaps between i odd and $i + 1$ even replicas after the next n_{swap} SR updates. This particular choice is purely one of convenience since it allows us to implement the swap updates on the different pairs of replicas in parallel.

The aim of using PT is to allow configurations of the ANN that have been trained at high temperature to be transferred with some probability to lower temperature, which can help lower temperature replicas to be bumped out of local minima of the training landscape. The PT approach becomes ineffective when the swap probability (Eq. (12)) between neighboring replicas is very low, effectively preventing replicas on one side of the temperature distribution from mixing with replicas on the other side. This problem can be mitigated by introducing additional replicas between the problematic temperatures and by optimizing the temperature distribution to avoid such bottlenecks.

Our strategy to optimize the temperature distribution is to pick an inverse-temperature distribution to ensure that we have equal swap probabilities between replicas [40, 41]. We propose to replace β_i for $i \in [1, n_R - 2]$ (excludes the lowest and highest temperatures) by:

$$\beta_i^* = \frac{1}{2} \left(\beta_i + \frac{\beta_{i-1}\bar{E}_- + \beta_{i+1}\bar{E}_+}{\bar{E}_- + \bar{E}_+} \right), \quad (13)$$

where $\bar{E}_- = \bar{E}_{i-1} - \bar{E}_i$, $\bar{E}_+ = \bar{E}_i - \bar{E}_{i+1}$. The update is accepted if $\beta_{i-1} > \beta_i^* > \beta_{i+1}$. The second term in the above expression arises from demanding that the probability of swapping between the $i - 1 \leftrightarrow i$ replicas (as defined in Eq. 12) and the $i \leftrightarrow i + 1$ replicas be equal, i.e.:

$$(\beta_{i-1} - \beta_i)(\bar{E}_{i-1} - \bar{E}_i) = (\beta_i - \beta_{i+1})(\bar{E}_i - \bar{E}_{i+1}). \quad (14)$$

To prevent rapid changes in the inverse-temperature β_i^* , we take an average of its current value β_i and the solution

to the above equation. Our approach is to first optimize the odd values of i followed by the even values [41].

III. RESULTS

A. Precipice problem

In order to illustrate the advantages afforded by optimizing the temperature distribution, we start by studying a toy model with a deep local minimum in its energy landscape. Our target Hamiltonian is given by the ‘‘Precipice problem’’ [42] with a uniform transverse field:

$$\hat{H} = \frac{1}{2}(1-s) \sum_{i=1}^n (\hat{\mathbf{1}} - \hat{\sigma}_i^x) + s \sum_{x \in \{0,1\}^{\otimes n}} f(x)|x\rangle\langle x|, \quad (15)$$

where $f(x)$ is a function that only depends on the Hamming weight of the n -bit string x and is given by:

$$f(x) = \begin{cases} -1 & \text{if } |x| = n \\ |x| & \text{otherwise} \end{cases}. \quad (16)$$

We pick $s = 4/5$ so that the Hamiltonian \hat{H} is dominated by the contribution from $f(x)$, which exhibits a local minimum at $x = 0$ that is a Hamming distance of n from the global minimum at $x = 2^n - 1$. The local minimum is pernicious because after initializing the wavefunction randomly the energy gradient calculated by SR pushes the ANN wavefunction towards the local minimum with high probability. Only if the wavefunction happens to start with a sufficient overlap with the global minimum will the wavefunction be pushed towards it with SR. Once in the local minimum, it is extremely unlikely to escape unless an appropriate escape mechanism such as PT is used [30].

The precipice model serves as a useful test case because we can easily eliminate the role of ANN expressibility and sampling from the effectiveness of the training and hence study the role played by PT. The Hamiltonian \hat{H} is qubit permutation invariant, and its ground state is symmetric under qubit permutations. Therefore, we can restrict the RBM ansatz to satisfy these conditions by having it depend only on the Hamming weight of the input x :

$$\psi_x(\alpha) = e^{\alpha \sum_{i=1}^n z_i} \prod_{\mu=1}^m \cosh \left(b_\mu + W_\mu \sum_{i=1}^n z_i \right), \quad (17)$$

which dramatically reduce the number of variational parameters to $1 + 2m$. This allows us to consider large choices of m with little computational cost to ensure the RBM is expressive enough to describe the ground state of \hat{H} . Furthermore, since all computational basis states with the same Hamming weight have the same amplitude, we can perform exact sampling *without* an exponential cost in the system size n . Details of the simulation settings are provided in Appendix A.

We study the case of $n = 32$ with a number of replicas n_R in the range $[6, 10]$. In our previous study [30], this number of replicas was insufficient to find the ground state for this system size, but as we show here becomes sufficient for $n_R \geq 7$ by optimizing the temperature distribution.

To demonstrate that the temperature optimization performs as expected, we show in Fig. 1 a running average of the swap probability calculated over 50 swap attempts. In Fig. 1(a), we see that in the case of no temperature optimization and with our choice of initial temperature distribution, there are pairs of replicas, specifically replica pairs (2,3) and (3,4), that exhibit effectively zero swap probability. This prevents configurations trained at higher temperatures to be exchanged with those at lower temperatures, and we do not observe a single case of finding the ground state with 50 independent simulations.

In contrast, in Fig. 1(b) we show how the swap probability for all pairs of replicas converges to a non-zero value. The exact non-zero value depends on the number of replicas used: a higher value is reached as more replicas are used. Unlike the case without temperature optimization, the algorithm is now able to find the ground state. For the particular case illustrated in Fig. 1(b), this coincides with a ‘blip’ in the swap probability between the 0 and 1 replicas, where the configuration at T_{\min} finds a lower energy and its configuration is swapped with the configuration at $T = 0$. This can be seen in Fig. 2(a) where the expectation value of the Hamiltonian for the zero temperature replica is shown to finally reach the ground state at that time.

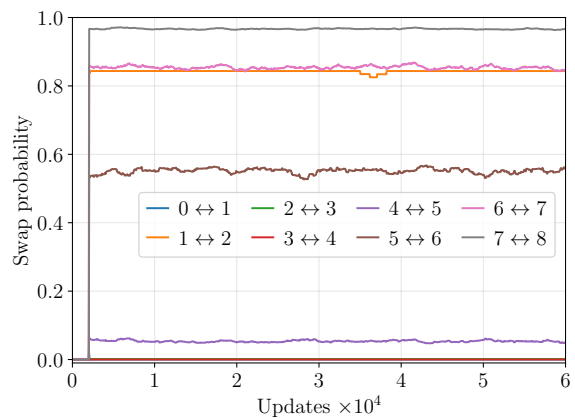
In Fig. 2(b), we show how the frequency of finding the ground state depends on the number of replicas. For 6 replicas and less, the swap probabilities are too low to allow the algorithm to find the ground state with the fixed number of updates we performed. As the number of replicas is increased, the number of updates needed to find the ground state is reduced, but the benefit of having more replicas diminishes once the swap probability becomes too large. This is consistent with what is observed in more ‘traditional’ studies using PT where an optimal swap probability is observed [43].

B. J_1 - J_2 Model with RBMs

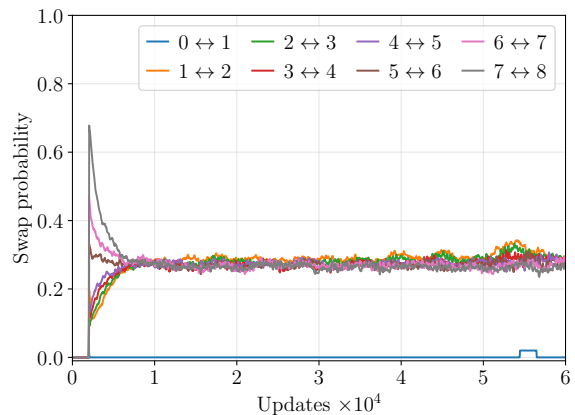
As a second test of our method, we study the J_1 - J_2 model on a square grid with open boundary conditions. The Hamiltonian of the system is given by:

$$\hat{H} = J_1 \sum_{\langle i,j \rangle} \vec{\sigma}_i \cdot \vec{\sigma}_j + J_2 \sum_{\langle\langle i,j \rangle\rangle} \vec{\sigma}_i \cdot \vec{\sigma}_j \quad (18)$$

where $\vec{\sigma}_i = \hat{\sigma}_i^x \hat{x} + \hat{\sigma}_i^y \hat{y} + \hat{\sigma}_i^z \hat{z}$ is the vector of Pauli operators acting on site i , $\langle i, j \rangle$ denotes nearest neighbor interactions, and $\langle\langle i, j \rangle\rangle$ denotes next nearest neighbor interactions. Because the Hamiltonian commutes with the total z -magnetization operator $\hat{M}^z = \sum_{i=1}^n \hat{\sigma}_i^z$, the energy



(a) Without optimization



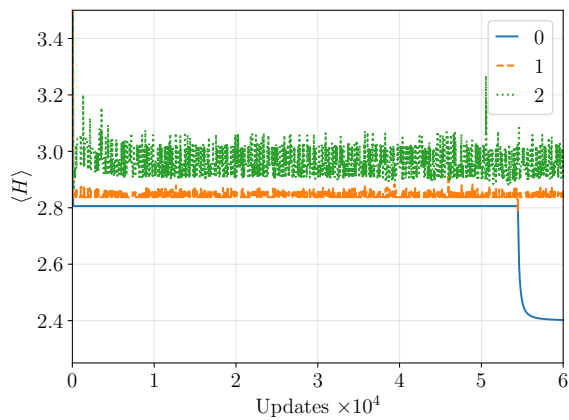
(b) With optimization

FIG. 1. Running average of the swap probability with 10 replicas for a single simulation (a) without temperature optimization and (b) with temperature optimization for the precipice problem. The running average is performed over 50 swap attempts (or equivalently 200 SR updates).

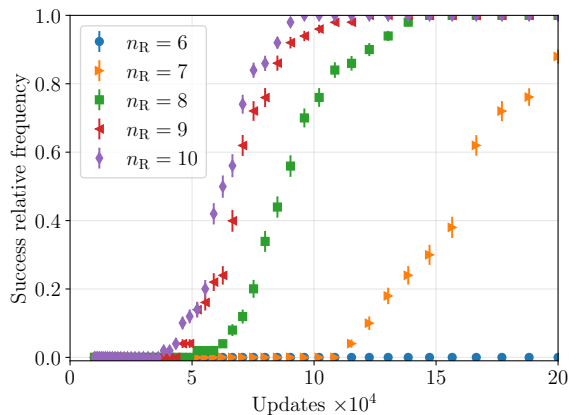
eigenstates can be expressed as simultaneous eigenstates of \hat{M}^z . For simplicity, we assume that the number of sites is even, in which case the ground state has is an eigenstate of \hat{M}^z with eigenvalue 0. This means we can restrict the Monte Carlo sampling in SR to computational basis states with Hamming weight $n/2$ configurations (or equivalently to spin configurations with an equal number of up and down spins).

For our first case, we focus on a 4×5 system with $J_1 = 1$ and $J_2 = 0.695$, training with an RBM. This is close to the point where the gap between the first excited state and ground state is smallest, near $J_2 = 0.7$, and where we find the greatest difficulty in training a RBM.

We use a RBM ansatz with $n = 20$ visible units and $m = 40$ hidden units for our variational wavefunction. This ansatz is likely not expressive enough to fully capture the ground state; we have not observed energies reaching the ground state in any of our simulations. However, it is expressive enough to capture states with en-



(a)



(b)

FIG. 2. (a) Expectation value of the precipice Hamiltonian (Eq. (15)) for the lowest three temperature replicas during training with $n_R = 10$ corresponding to the simulation in Fig. 1(b), which includes temperature optimization. (b) Frequency of finding the ground state with temperature optimization for the precipice problem. The results are calculated for 50 independent simulations, with the error bars corresponding to the 2σ confidence interval calculated using a bootstrap.

ergies below the first excited state, which we term as success throughout the rest of this section.

The initial temperature distribution is picked to be $T_k = T_{\min} + (T_{\max} - T_{\min}) \left(\frac{k-1}{n_R-2}\right)^3$, where $k = 1, \dots, n_R - 1$. We initialize with the parameter choices $T_{\min} = 0.1$ and $T_{\max} = 20$. We give further details of our simulation settings in Appendix B 1.

In Fig. 3(a) we measure the likelihood of reaching an energy below the first excited state with a single replica and with PT with 6 replicas. In the case of PT, we consider the two cases of allowing temperature optimization throughout the training and holding the temperature fixed throughout the training. The J_1 - J_2 problem is inherently difficult for a single replica RBM system to solve without any PT, with a success rate of only $3\% \pm$

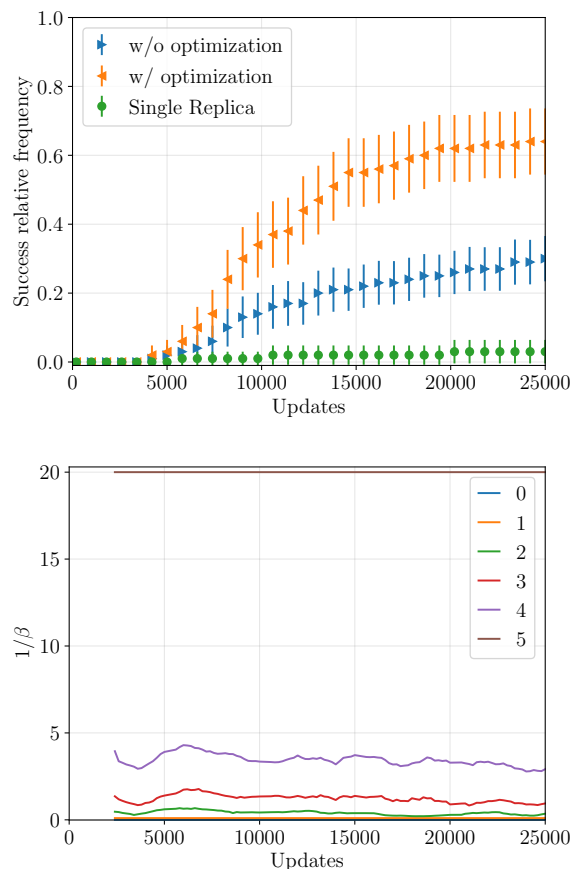


FIG. 3. (a) Relative frequency of finding an energy below the first excited state (-34.70212) of the open boundary condition 4×5 J_1 - J_2 problem at $J_2 = 0.695$ with increasing number of updates in PT for 100 independent simulations, with the error bars corresponding to the 2σ confidence interval calculated using twice the standard error of the mean. For the PT simulations (\triangleleft and \triangleright data points) we use $n_R = 6$ replicas. (b) The running average value of β as a function of updates for a representative run when the temperature is allowed to adjust.

3% after 2.5×10^4 updates. PT without any temperature optimization improves the overall success rate to $30\% \pm 9\%$, demonstrating a clear improvement. Once we allow for temperature optimization, we achieve a significantly higher success rate of $65\% \pm 9\%$. In Fig. 3(b), we show how the temperature $1/\beta$ changes over time for a typical run where we allow the temperatures to optimize. We find that our initial polynomial distribution of temperatures is relatively good and only small adjustments are made throughout the run. This demonstrates that optimizing temperatures can increase success probability even for systems that are initially well tuned.

The reason for this improvement can be seen by examining the swap probabilities between each of the different replicas for a typical run, as shown in Fig. 4. When the temperatures are allowed to optimize, the swap probabilities converge near 0.3, although the values are still noisy due to the limited sample size and number of updates.

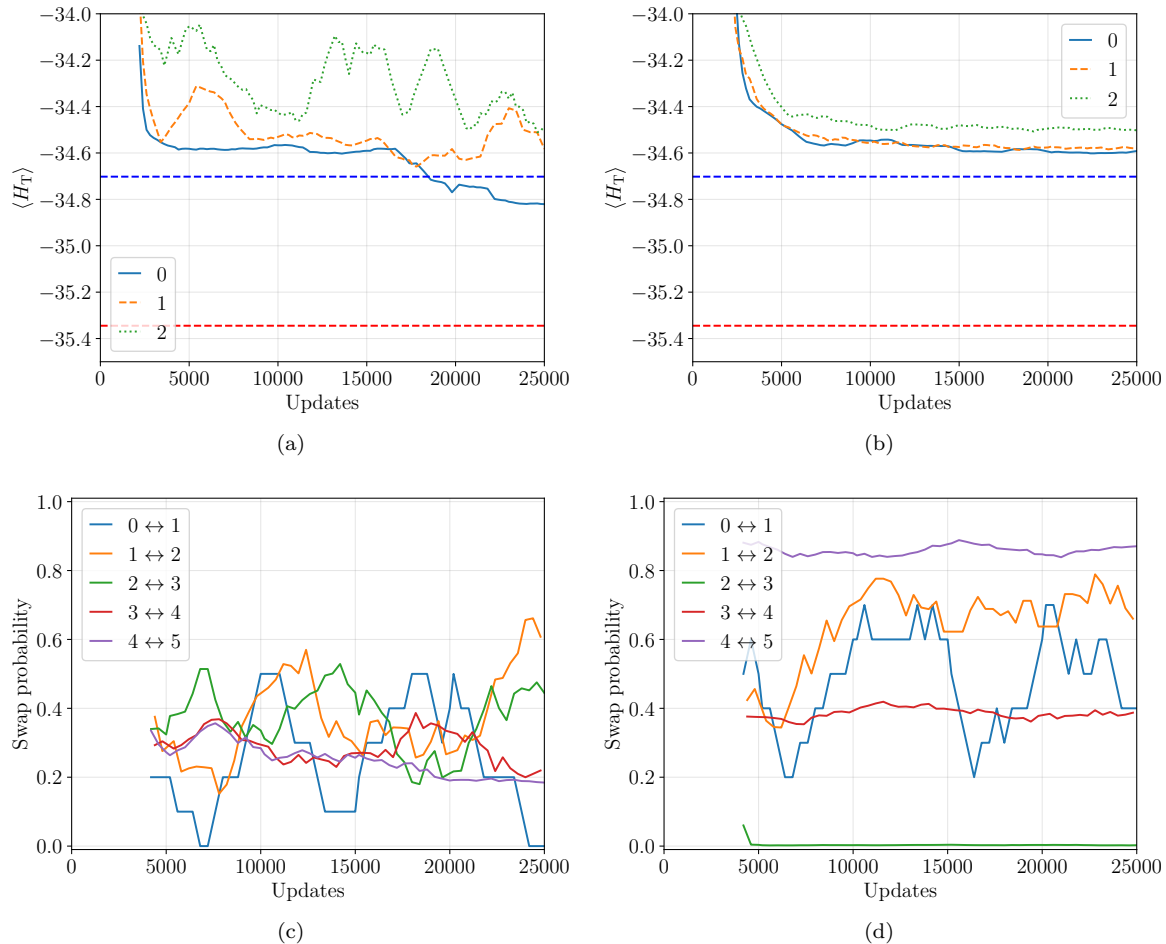


FIG. 4. The running average of the energy of the first 3 replicas for a representative run of the open boundary conditions 4×5 J_1 - J_2 model where the temperatures are (a) allowed to adjust and (b) held fixed. The red dashed line corresponds to the ground state energy (-35.34479) and the blue dashed line to the first excited state energy (-34.70212). The running average of the probability of swapping between different replicas for the corresponding run for the case of (c) allowing the temperature to adjust and (d) holding the temperatures fixed.

For transferring into the zero replica (which contains the pure target Hamiltonian), the probability of swapping is a binary 0 or 1, based on whether replica 1 has a lower target energy. When we take the running average in Fig. 4(c), this corresponds to the averaged probability moving up for update regions where there is more transfer into the zero replica. This move toward high probabilities for swapping into/out of the zero replica is particularly pronounced at 10^4 updates and 1.6×10^4 updates. The latter of these update states corresponds precisely with when the energy of the zero replica begins to lower, eventually dipping below the first excited state. In contrast, when the temperatures are not allowed to optimize as in Fig. 4(d), the probabilities of swapping never converge toward any value. Furthermore, the probability of swapping between the 2nd and 3rd replicas remains at essentially 0 throughout the entirety of the simulation. This leads to an inability for any configurations from replicas 3 to 5 to ever make their way to the 0 replica, which likely

leads to the simulation never reaching energies below the first excited state. While these results are for two specific runs of PT for this problem, they are representative for how the algorithm achieves success for a majority of our simulations. This shows that optimizing temperatures allows the PT algorithm to perform better by ensuring that states are mixed in from the higher temperatures in the distribution at a steady rate.

We further find that the temperature optimization algorithm is relatively robust to the initial choice of temperature distribution. In Fig. 5, we explore a linear initial distribution of temperatures, $T_k = T_{\min} + (T_{\max} - T_{\min}) \left(\frac{k-1}{n_R-2} \right)$, where $k = 1, \dots, n_R - 1$. The probability of success at $J_2 = 0.695$ nearly exactly matches what we see for the polynomial distribution in Fig. 3(a). Without optimizing the temperatures, we see a success rate of 0.22 ± 0.082 . Once we allow the temperatures to optimize, the success rate improves to 0.68 ± 0.093 . In

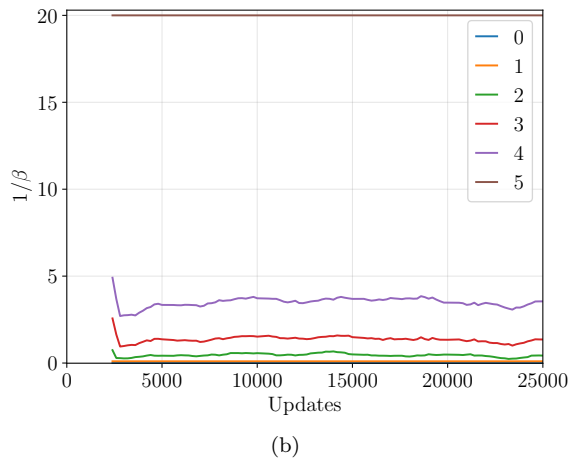
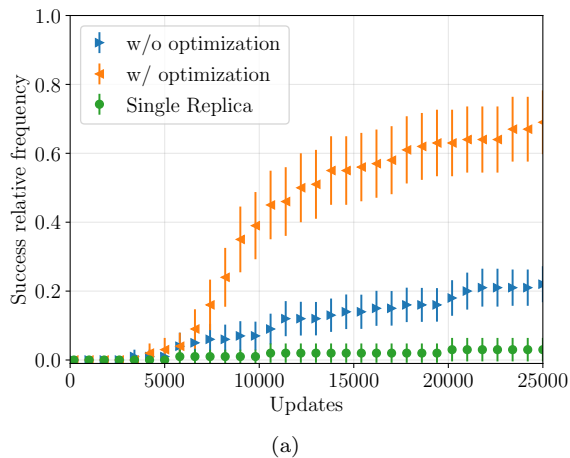


FIG. 5. (a) Relative frequency of finding an energy below the first excited state (-34.70212) of the open boundary condition 4×5 J_1 - J_2 problem at $J_2 = 0.695$ when starting from an initial linear temperature distribution instead of a polynomial distribution over 100 independent runs, with the error bars corresponding to the 2σ confidence interval calculated using twice the standard error of the mean. (b) The running average value of β as a function of updates for a representative run when the temperature is allowed to adjust.

Fig. 5(b), the β values in a representative example run adjust significantly away from their initial linear distribution within just approximately 10^3 updates. This distribution of temperatures closely matches the distribution that we see when starting with an initially polynomial distribution. From these results we conclude that our algorithm is robust to choices of the initial temperature distributions.

We do however observe a relatively strong dependence on the choice of minimum and maximum temperatures, which are held fixed throughout the simulation. In Fig. 6, we vary the maximum temperature T_{\max} for a system with $n_R = 6$ and an initial polynomial distribution of temperatures and note how the success rate changes. We see that for maximum temperatures greater ≥ 10 , the success rate for simulations where the temperature dis-

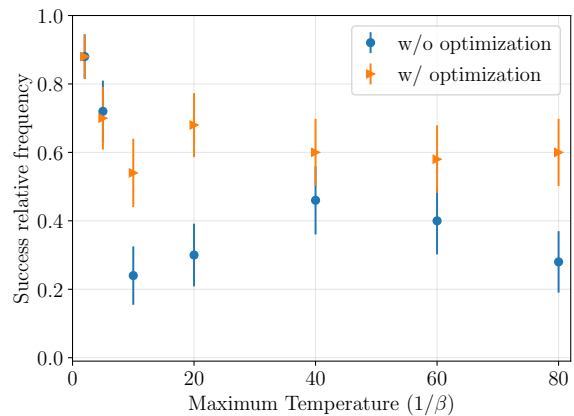


FIG. 6. Relative frequency of finding an energy below the first excited state of the open boundary condition 4×5 J_1 - J_2 problem as a function of the maximum temperature.

tribution is optimized holds steady at ≈ 0.60 . For simulations without temperature optimization, the success rate varies from ≈ 0.20 to 0.40 . Since setting the maximum temperature also affects the initial temperature distribution, this variation is expected.

However as the maximum temperature decreases below 10, the success rate for the simulations drastically increases, with a choice of $T_{\max} = 2$ giving a success rate of 0.88 for both simulations with and without temperature optimization. This shows that the choice of $T_{\max} = 20$ explored in the earlier figures was not optimal for maximizing success. Therefore the success frequency of our algorithm is still highly sensitive to the initial choice of the maximum temperature. Nevertheless, the temperature optimization does provide robust improvement to the success rate even for suboptimal choices of initial temperature, which can speed up the process of finding viable solutions. Future work will focus on automating the selection of the T_{\max} parameter.

In Appendix C, we explore the dependence of our algorithm's performance on the choice of additional hyperparameters such as the number of replicas and the number of samples. We find that the performance can depend strongly on these values. Nonetheless, in all cases tested, allowing the temperatures to optimize within the simulation provides at least as much success as systems without optimization, and typically substantially improves success rates for minimal additional computational cost.

C. J_1 - J_2 Model with Feedforward Networks

As a final test, we study the J_1 - J_2 on a square lattice with periodic boundary conditions for a 6×6 system. In this case, we choose $J_1 = 1$ and $J_2 = 0.62$. This is close to the point where the energy gap between the first excited state and the ground state is smallest, near $J_2 = 0.58$. For this study, we use a three-layer feedfor-

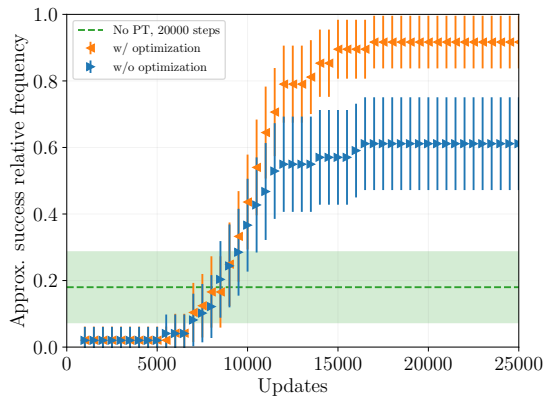


FIG. 7. Success relative frequency on the 6×6 J_1 - J_2 model with $J_2 = 0.62$ using a feedforward network with $(48, 24, 24)$ hidden units over 50 independent runs. The green dashed line corresponds to the success frequency of independent single-replica runs (without PT) after 2×10^4 updates with the shaded region corresponding to the 2σ confidence interval calculated using a bootstrap. The blue triangles correspond to PT with 5 replicas without temperature optimization, and the orange triangles correspond to PT with 5 replicas with temperature optimization. Success is defined as finding a state with an average energy that is at least one standard error below the first excited of -70.07405 . The error bars correspond to the 2σ confidence interval calculated using a bootstrap.

ward neural network instead of a RBM, and we denote the number of hidden nodes in each layer by (h_1, h_2, h_3) . This network is more expressive than the RBMs used in Sec. III B and is intended to test our method on a more expressive architecture. For this system size, exact sampling is computationally prohibitive and prevents us from evaluating the energy of the NQS exactly, so we employ a different criterion to define success. We take a running mean of the energy and standard deviation over 50 steps and if the average energy reported is beneath -70.07405 (computed using DMRG [44–47] with a bond dimension of 2048), by more than a third of the mean standard deviation, we freeze the parameters and sample at that step for 10^3 steps with 1024 samples each. Each of these sampling runs gives a sample mean energy and a sample standard deviation, from which we can calculate a mean of the means energy and a standard error of the mean. If the mean of the mean energies is one standard error below the first excited state energy, then we flag the simulation as a possible success. When the simulation terminates we again sample, this time for 10^3 steps with 512 samples each in order to confirm the success of the simulation. We find that all simulations that are flagged successful at intermediate points in the simulation are confirmed successful with this final test.

For our three-layer feedforward network, we choose a network structure such that the first hidden layer has twice the hidden units as the next two hidden layers, and we choose $(h_1, h_2, h_3) = (48, 24, 24)$. We find this is

expressive enough to yield states with energies below the first excited state.

For the PT runs, we use a linear initial temperature distribution: $T_k = T_{\min} + (T_{\max} - T_{\min}) \left(\frac{k-1}{n_R-2} \right)$. We do this to highlight the adaptivity of the temperature optimization scheme. We start performing replica swaps after the 10^3 -th SR update step when energies have had time to converge, after which we perform 10^2 SR update steps between replica swaps and temperature updates. Some of the implementation details of the variational algorithm used for the feedforward network are different from those of Sec. III B, and we give these details in Appendix B 2.

We show the success of PT using the $(48, 24, 24)$ feedforward network in Fig. 7. We observe a clear advantage to using PT over not using PT in terms of success frequency, and we also begin to see a separation between the simulations with and without temperature optimization after approximately 10^4 update steps. After 1.5×10^4 steps, the increase in success rate for the case without temperature optimization slows down and possibly saturates near 60%, suggesting that the system can get stuck in local minima. This is in contrast to the case with temperature optimization where a properly tuned temperature distribution can help it escape from such local minima and succeed with a rate near 90%.

IV. CONCLUSIONS

In this work, we demonstrated the impact of the replica temperature distribution on the effectiveness of PT to help train an ANN to represent a low-energy quantum state. Training with PT already shows increased success rates over training with a single replica, and by adaptively adjusting the temperature distribution such that all pairs of replicas swap with equal probability we reach even higher success frequencies at quicker rates with negligible computational cost. We attribute this improvement to better escape rates from local minima. These results are more pronounced for problems where the training is difficult. This can arise from deep local minima in the energy potential, which was illustrated by the Precipice problem, but also when the number of parameters gets larger for more expressive networks, as was demonstrated by our different network sizes for the 6×6 J_1 - J_2 model. We expect that the difficulties encountered for the J_1 - J_2 problem will only be exacerbated at larger problem sizes, so we can expect temperature optimization to be crucial in that case.

We have focused on neural networks that are generic to demonstrate the effectiveness of our proposed methodology. Replacing the RBM or feedforward networks with more state-of-the-art networks adopted for NQS such as GCNN’s [18, 19] is straightforward. We expect the advantages of PT to arise when the training is stymied by local minima from which the variational algorithm is slow to escape, and the PT replica swaps provide a mechanism

for escape, for which optimizing the temperature distribution is important to be effective.

An important feature of the approach we advocate is that it introduces minimal additional computational cost to the PT algorithm, and in all the cases we have studied, optimizing the temperature distribution improves the performance of the PT algorithm or at least provides equal performance. It introduces only two additional hyperparameters, the minimum and maximum temperature of the distribution, and we leave automating these hyperparameters for future work.

ACKNOWLEDGMENTS

We would like to thank the UNM Center for Advanced Research Computing, supported in part by the National Science Foundation, for providing the high performance computing resources used in this work.

This material is based upon work supported by the National Science Foundation under grant number 2037755. This material is based upon work supported by the Air Force Office of Scientific Research under award number

FA9550-22-1-0498. Any opinions, findings, and conclusions or recommendations expressed in this material are those of the author(s) and do not necessarily reflect the views of the United States Air Force.

This work was performed, in part, at the Center for Integrated Nanotechnologies, an Office of Science User Facility operated for the U.S. Department of Energy (DOE) Office of Science.

This article has been co-authored by an employee of National Technology & Engineering Solutions of Sandia, LLC under Contract No. DE-NA0003525 with the U.S. Department of Energy (DOE). The employee owns all right, title and interest in and to the article and is solely responsible for its contents. The United States Government retains and the publisher, by accepting the article for publication, acknowledges that the United States Government retains a non-exclusive, paid-up, irrevocable, world-wide license to publish or reproduce the published form of this article or allow others to do so, for United States Government purposes. The DOE will provide public access to these results of federally sponsored research in accordance with the DOE Public Access Plan <https://www.energy.gov/downloads/doe-public-access-plan>.

-
- [1] A. Kitaev, A. Shen, and M. Vyalyi, *Classical and Quantum Computation*, Graduate studies in mathematics, Vol. 47 (American Mathematical Society, 2002).
 - [2] J. Kempe and O. Regev, 3-local hamiltonian is qma-complete, *Quantum Info. Comput.* **3**, 258 (2003).
 - [3] J. Kempe, A. Kitaev, and O. Regev, The complexity of the local hamiltonian problem, *SIAM Journal on Computing* **35**, 1070 (2006).
 - [4] B. O’Gorman, S. Irani, J. Whitfield, and B. Fefferman, Electronic Structure in a Fixed Basis is QMA-complete, *arXiv e-prints*, [arXiv:2103.08215](https://arxiv.org/abs/2103.08215) (2021).
 - [5] Y. Huang, Two-dimensional local hamiltonian problem with area laws is qma-complete, *Journal of Computational Physics*, [110534](https://arxiv.org/abs/110534) (2021).
 - [6] N. Astrakhantsev, T. Westerhout, A. Tiwari, K. Choo, A. Chen, M. H. Fischer, G. Carleo, and T. Neupert, Broken-symmetry ground states of the heisenberg model on the pyrochlore lattice, *Phys. Rev. X* **11**, 041021 (2021).
 - [7] M. Wilson, N. Gao, F. Wudarski, E. Rieffel, and N. M. Tubman, Simulations of state-of-the-art fermionic neural network wave functions with diffusion Monte Carlo, *arXiv e-prints*, [arXiv:2103.12570](https://arxiv.org/abs/2103.12570) (2021).
 - [8] Y. Nomura and M. Imada, Dirac-type nodal spin liquid revealed by refined quantum many-body solver using neural-network wave function, correlation ratio, and level spectroscopy, *Phys. Rev. X* **11**, 031034 (2021).
 - [9] A. Lovato, C. Adams, G. Carleo, and N. Rocco, Hidden-nucleons neural-network quantum states for the nuclear many-body problem, *Phys. Rev. Res.* **4**, 043178 (2022).
 - [10] W. Ren, W. Fu, X. Wu, and J. Chen, Towards the ground state of molecules via diffusion monte carlo on neural networks, *Nature Communications* **14**, 1860 (2023).
 - [11] T. Zhao, J. Stokes, and S. Veerapaneni, Scalable neural quantum states architecture for quantum chemistry, *Machine Learning: Science and Technology* **4**, 025034 (2023).
 - [12] Y.-T. Zhou, Z.-W. Zhou, and X. Liang, Solving fermi-hubbard-type models by tensor representations of back-flow corrections, *Phys. Rev. B* **109**, 245107 (2024).
 - [13] R. Rende, S. Goldt, F. Becca, and L. Loris Viteritti, Fine-tuning Neural Network Quantum States, *arXiv e-prints*, [arXiv:2403.07795](https://arxiv.org/abs/2403.07795) (2024).
 - [14] S. Sorella, Green function monte carlo with stochastic reconfiguration, *Phys. Rev. Lett.* **80**, 4558 (1998).
 - [15] S. Sorella, Generalized lanczos algorithm for variational quantum monte carlo, *Phys. Rev. B* **64**, 024512 (2001).
 - [16] A. Chen and M. Heyl, Empowering deep neural quantum states through efficient optimization, *Nature Physics* **20**, 1476 (2024).
 - [17] G. Carleo and M. Troyer, Solving the quantum many-body problem with artificial neural networks, *Science* **355**, 602 (2017).
 - [18] C. Roth and A. H. MacDonald, Group Convolutional Neural Networks Improve Quantum State Accuracy, *arXiv e-prints*, [arXiv:2104.05085](https://arxiv.org/abs/2104.05085) (2021).
 - [19] C. Roth, A. Szabó, and A. H. MacDonald, High-accuracy variational monte carlo for frustrated magnets with deep neural networks, *Phys. Rev. B* **108**, 054410 (2023).
 - [20] Z.-A. Jia, B. Yi, R. Zhai, Y.-C. Wu, G.-C. Guo, and G.-P. Guo, Quantum neural network states: A brief review of methods and applications, *Advanced Quantum Technologies* **2**, 1800077 (2019).
 - [21] H. Lange, A. Van de Walle, A. Abedinnia, and A. Bohrdt, From Architectures to Applications: A Review of Neural Quantum States, *arXiv e-prints*, [arXiv:2402.09402](https://arxiv.org/abs/2402.09402)

- (2024).
- [22] M. Medvidović and J. R. Moreno, Neural-network quantum states for many-body physics, *The European Physical Journal Plus* **139**, 631 (2024).
- [23] X. Liang, M. Li, Q. Xiao, J. Chen, C. Yang, H. An, and L. He, Deep learning representations for quantum many-body systems on heterogeneous hardware, *Machine Learning: Science and Technology* **4**, 015035 (2023).
- [24] T. Westerhout, N. Astrakhantsev, K. S. Tikhonov, M. I. Katsnelson, and A. A. Bagrov, Generalization properties of neural network approximations to frustrated magnet ground states, *Nature Communications* **11**, 1593 (2020).
- [25] A. Szabó and C. Castelnovo, Neural network wave functions and the sign problem, *Phys. Rev. Res.* **2**, 033075 (2020).
- [26] M. Bukov, M. Schmitt, and M. Dupont, Learning the ground state of a non-stoquastic quantum Hamiltonian in a rugged neural network landscape, *SciPost Phys.* **10**, 147 (2021).
- [27] R. H. Swendsen and J.-S. Wang, Replica monte carlo simulation of spin-glasses, *Phys. Rev. Lett.* **57**, 2607 (1986).
- [28] C. J. Geyer, Parallel tempering, in *Computing Science and Statistics Proceedings of the 23rd Symposium on the Interface*, edited by E. M. Keramidas and S. M. Kaufman (American Statistical Association, New York, 1991) p. 156.
- [29] K. Hukushima and K. Nemoto, Exchange monte carlo method and application to spin glass simulations, *Journal of the Physical Society of Japan* **65**, 1604 (1996).
- [30] T. Albash, C. Smith, Q. Campbell, and A. D. Baczewski, Quantum-inspired tempering for ground state approximation using artificial neural networks, *SciPost Phys.* **14**, 121 (2023).
- [31] H. G. Katzgraber, S. Trebst, D. A. Huse, and M. Troyer, Feedback-optimized parallel tempering monte carlo, *Journal of Statistical Mechanics: Theory and Experiment* **2006**, P03018 (2006).
- [32] P. Smolensky, Information Processing in Dynamical Systems: Foundations of Harmony Theory, in *Parallel Distributed Processing, Volume 1: Explorations in the Microstructure of Cognition: Foundations* (The MIT Press, 1986).
- [33] G. E. Hinton, Training Products of Experts by Minimizing Contrastive Divergence, *Neural Computation* **14**, 1771 (2002).
- [34] K. Hornik, M. Stinchcombe, and H. White, Multilayer feedforward networks are universal approximators, *Neural Networks* **2**, 359 (1989).
- [35] D. Hendrycks and K. Gimpel, Gaussian Error Linear Units (GELUs), *arXiv e-prints*, arXiv:1606.08415 (2016).
- [36] G. Carleo, K. Choo, D. Hofmann, J. E. T. Smith, T. Westerhout, F. Alet, E. J. Davis, S. Efthymiou, I. Glasser, S.-H. Lin, M. Mauri, G. Mazzola, C. B. Mendl, E. van Nieuwenburg, O. O'Reilly, H. Théveniaut, G. Torlai, F. Vicentini, and A. Wietek, Netket: A machine learning toolkit for many-body quantum systems, *SoftwareX*, 100311 (2019).
- [37] F. Vicentini, D. Hofmann, A. Szabó, D. Wu, C. Roth, C. Giuliani, G. Pescia, J. Nys, V. Vargas-Calderón, N. Astrakhantsev, and G. Carleo, NetKet 3: Machine Learning Toolbox for Many-Body Quantum Systems, *SciPost Phys. Codebases*, 7 (2022).
- [38] J. Bradbury, R. Frostig, P. Hawkins, M. J. Johnson, C. Leary, D. Maclaurin, G. Necula, A. Paszke, J. VanderPlas, S. Wanderman-Milne, and Q. Zhang, *JAX: composable transformations of Python+NumPy programs* (2018).
- [39] M. Hibat-Allah, R. G. Melko, and J. Carrasquilla, Supplementing Recurrent Neural Network Wave Functions with Symmetry and Annealing to Improve Accuracy, *arXiv e-prints*, arXiv:2207.14314 (2022).
- [40] K. Hukushima, Domain-wall free energy of spin-glass models: Numerical method and boundary conditions, *Phys. Rev. E* **60**, 3606 (1999).
- [41] I. Rozada, M. Aramon, J. Machta, and H. G. Katzgraber, Effects of setting temperatures in the parallel tempering monte carlo algorithm, *Phys. Rev. E* **100**, 043311 (2019).
- [42] W. van Dam, M. Mosca, and U. Vazirani, How powerful is adiabatic quantum computation?, in *Proceedings 42nd IEEE Symposium on Foundations of Computer Science* (2001) pp. 279–287.
- [43] A. Kone and D. A. Kofke, Selection of temperature intervals for parallel-tempering simulations, *The Journal of Chemical Physics* **122**, 206101 (2005).
- [44] S. R. White, Density matrix formulation for quantum renormalization groups, *Phys. Rev. Lett.* **69**, 2863 (1992).
- [45] S. R. White, Density-matrix algorithms for quantum renormalization groups, *Phys. Rev. B* **48**, 10345 (1993).
- [46] U. Schollwöck, The density-matrix renormalization group, *Rev. Mod. Phys.* **77**, 259 (2005).
- [47] U. Schollwöck, The density-matrix renormalization group in the age of matrix product states, *Annals of Physics* **326**, 96 (2011), january 2011 Special Issue.
- [48] S.-C. T. Choi and M. A. Saunders, Algorithm 937: Minres-qlp for symmetric and hermitian linear equations and least-squares problems, *ACM Trans. Math. Softw.* **40** (2014).
- [49] M. Schmitt and M. Heyl, Quantum many-body dynamics in two dimensions with artificial neural networks, *Phys. Rev. Lett.* **125**, 100503 (2020).

Appendix A: Simulation settings for precipice problem

For the simulations on the Precipice problem discussed in Sec. III A, we use SR with an adaptive learning rate. This requires solving the linear system of equations in Eq. (10). To do this, we first perform an explicit regularization of s by replacing its diagonal elements by [17]:

$$s_{kk} \rightarrow s_{kk}(1 + \lambda(p)) \quad (\text{A1})$$

where p is the current update step and we choose $\lambda(p) = \max(\lambda_0 b^p, \lambda_{\min})$ with $\lambda_0 = 100$, $b = 0.9$, $\lambda_{\min} = 10^{-4}$. We then use MINRES-QLP [48] to solve the equations, using a tolerance of 10^{-6} and a maximum of 10^3 iterations. The total number of SR updates in the simulation is 2×10^5 .

The learning rate η in Eq. (10) is adjusted adaptively using a Heun second order consistent integrator [49] with an error of 10^{-8} . For PT, the lowest finite temperature in the simulation is given by $T_1 = 0.05$ and the largest temperature is given by $T_{n_{\text{nr}}-1} = 10$. PT swaps are performed at every $n_{\text{swap}} = 20$ updates, alternating between odd and even neighbors as discussed in the main text. The initial temperature distribution is

picked to be $T_k = T_{\min} + (T_{\max} - T_{\min}) \left(\frac{k-1}{n_R-2}\right)^3$, where $k = 1, \dots, n_R - 1$. In the case of optimizing the temperature distribution, the update of the temperature distribution occurs every 200 updates.

Appendix B: Simulation settings for the J_1 - J_2 problem

1. RBM settings

For the simulations for the 4×5 J_1 - J_2 problem using the RBM shown in the main text, we use a similar procedure as discussed in Appendix A. We use MINRES-QLP with the same tolerance and maximum number of updates. We use the same SR with an adaptive learning rate implementation but now with an allowed error of 10^{-5} .

Because the ground state is in the zero-magnetization sector, we restrict our Monte Carlo sampling to computational basis states with fixed Hamming weight equal to 10. We take 200 samples per SR update step, which are used to estimate the quantities f and s in Eq. (11). We also use these samples to calculate the running average of the energy used in calculating the parallel tempering probabilities (Eq. (12)) as well as the temperature updates (Eq. (13)). For the plots of the energy in Fig 4, we calculate the energy of each replica exactly by sampling all Hamming weight 10 states, but the exact energy is not used in the training in any way. When optimizing the temperatures, we start with 400 updates of “burn in” after which we update the temperature distribution every 200 updates. PT swaps are performed at every $n_{\text{swap}} = 100$ updates, alternating between odd and even neighbors as discussed in the main text. For all these simulations, we use a total of 25000 updates.

We discuss the sensitivity of our results to some of the parameter choices in Appendix C.

2. Feedforward Network Settings

The results for the feedforward neural networks in Sec. III C were obtained using the python package NetKet [37]. This package can handle arbitrary neural network architectures and uses autodifferentiation implemented with JAX [38]. We have used NetKet’s default version of SR, which uses the conjugate gradient method to perform the inversion in Eq. (10).

In contrast to the RBM simulations which use a Heun second order consistent integrator as well as SR to provide accurate gradients, we have used SR alone here. We expect an adaptive learning rate would be useful on this larger system, but it is more computationally expensive. We choose a learning rate of 10^{-3} and train for 10^4 total steps in the case of the largest feedforward network and 2.5×10^4 steps for the two smaller feedforward networks.

Parallel tempering updates do not begin until step 10^3 to allow the optimization time to converge. After this, we swap replicas and perform temperature optimization (if indicated) every 10^2 steps.

Appendix C: Hyperparameter dependence in the J_1 - J_2 problem

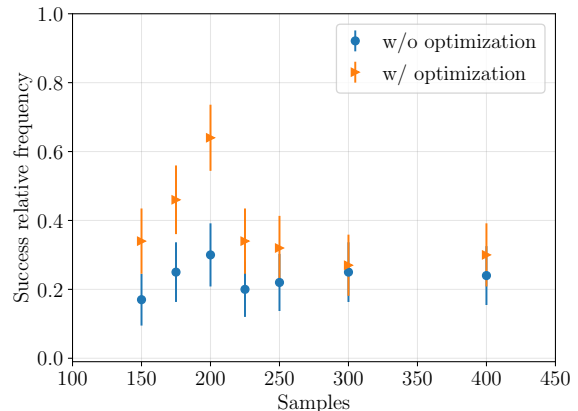
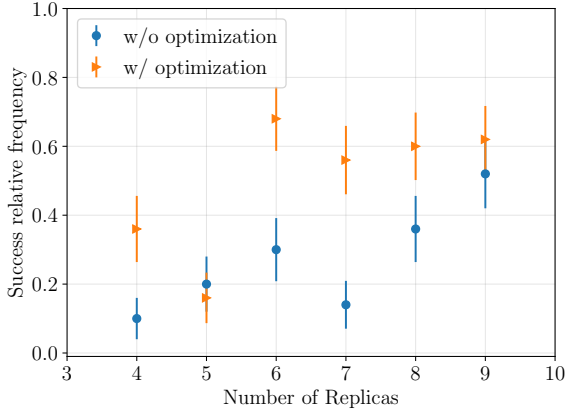


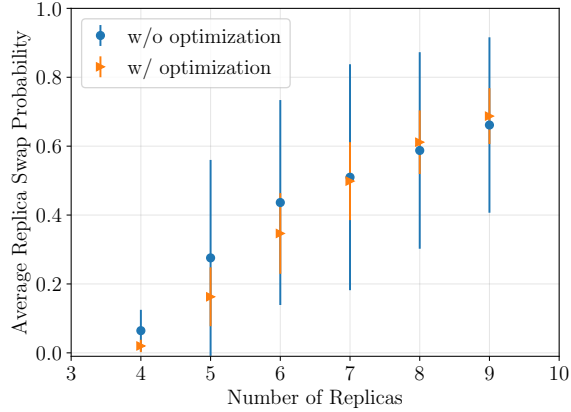
FIG. 8. Relative frequency of finding an energy below the first excited state of the open boundary condition 4×5 J_1 - J_2 problem when varying the number of samples taken over 100 independent runs, with the error bars corresponding to the 2σ confidence interval calculated using twice the standard error of the mean.

While optimizing temperatures of PT does lead to improved performance for the J_1 - J_2 problem, the degree of improvement is highly dependent on the choice of hyperparameters. In this section, we further examine the 4×5 J_1 - J_2 model using an RBM architecture to determine the dependence of the final results on the hyperparameter choices.

We first explore how the PT algorithm performs as the number of samples used to estimate the next update increases in Fig. 8. As the success rate increases from 150 to 200 samples, the success rate steadily increases from 0.34 ± 0.095 to 0.64 ± 0.096 when the temperatures are allowed to optimize, and from 0.17 ± 0.075 to 0.30 ± 0.091 when the temperatures are held constant. The ratio of improvement remains about a factor of 2 in all of these cases. However, the success rate peaks dramatically at 200 samples both with and without temperature optimization. The success rate for larger sample sizes tends to saturate with a rate of 0.30 ± 0.091 when optimizing the temperatures and 0.24 ± 0.085 without optimizing temperatures at 400 samples. We hypothesize that this peak at 200 samples is due to the finite samples providing beneficial noise that allows certain replicas to bump out of local minima. As the sample size increases, this noise is reduced, and it becomes harder to escape the local minima.



(a)



(b)

FIG. 9. (a) Relative frequency of finding an energy below the first excited state (-34.70212) of the open boundary condition 4×5 J_1 - J_2 problem when varying the number of replicas over 10^2 independent runs, with the error bars corresponding to the 2σ confidence interval calculated using twice the standard error of the mean. (b) The average swap probability between replicas at the end of each run.

Finally, we also investigate varying the number of replicas within the PT algorithm in Fig. 9. We find a strong peak in the success rate when allowing the temperatures to optimize at 6 replicas. Beyond this point the success rate generally seems to saturate near 0.60 when the temperature is allowed to optimize. The success rate for cases where the temperature is not optimized also slowly increases to nearly match the adjusting temperature rate, demonstrating that as more temperatures are covered, the benefits of optimizing the temperature become less strong.

However, we do see more variable success rate results around 4 and 5 replicas, with 4 replicas seeing a spike in success rate when temperatures are allowed to optimize. This may be related to an optimum average swap probability, as shown in Fig. 9(b). As the number of replicas increases, the average swap probability increases relatively linearly for both cases where the temperature is allowed to optimize and cases where it is not. The spread of the probabilities is much narrower when the temperatures are allowed to optimize, however, confirming that the optimization algorithm is leading to a degree of convergence in the swap probability. Probabilities around 0.20 have previously been associated with optimum success probabilities in similar PT algorithms [43]. In our work, the optimum probability of swapping appears to be around 0.40 for the 6 replica case. This higher rate of swapping may be related to the limited number of samples and total updates performed in this work.

Taken together, these results show that the overall success rate of our PT algorithm for ground state discovery is, to a certain extent, dependent on the hyperparameters used within the simulation. Nevertheless, in all cases studied, optimizing the temperature does improve the performance of the PT algorithm, or at least provides equal performance with minimal additional computational cost. Furthermore, it can often significantly reduce the needed computational cost by providing high success rates at lower numbers of samples and replicas.